A discrete subset of epigenetically primed human NK cells mediates antigen-specific immune responses

Victoria Stary[1], Ram Vinay Pandey[2], Johanna Strobl[2], Lisa Kleissl[2,3], Patrick Starlinger[1,4], David Pereyra[1,5], Wolfgang Weninger[2], Gottfried F. Fischer[6], Christoph Bock[7,8], Matthias Farlik[2,#], Georg Stary[2,3,7,#,*]

Supplementary Materials

Supplementary Figure 1.

a Single cell RNA-seq on liver CD45+ cells superimposed with expression patterns of known marker genes for ILC subtype characterization

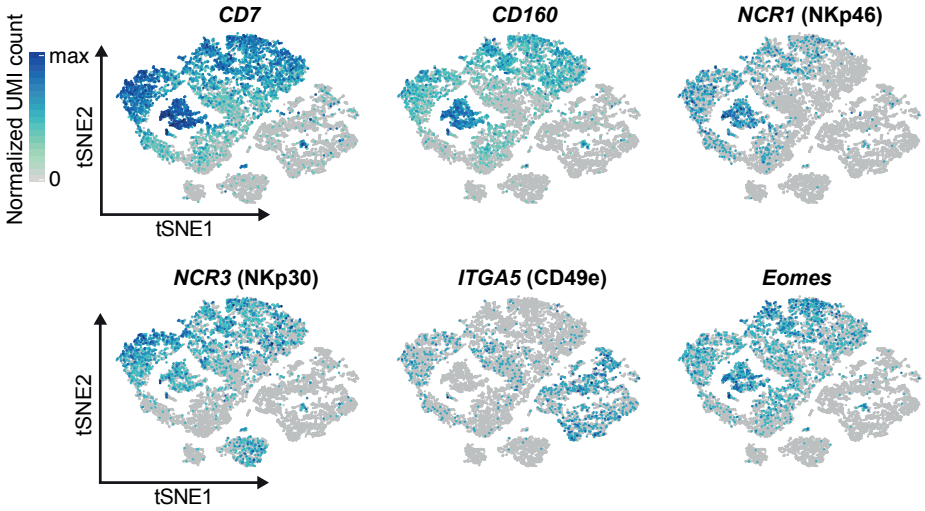

b Representative dot plots NK cells with anti-CD49a, anti-CD16 and isotype control

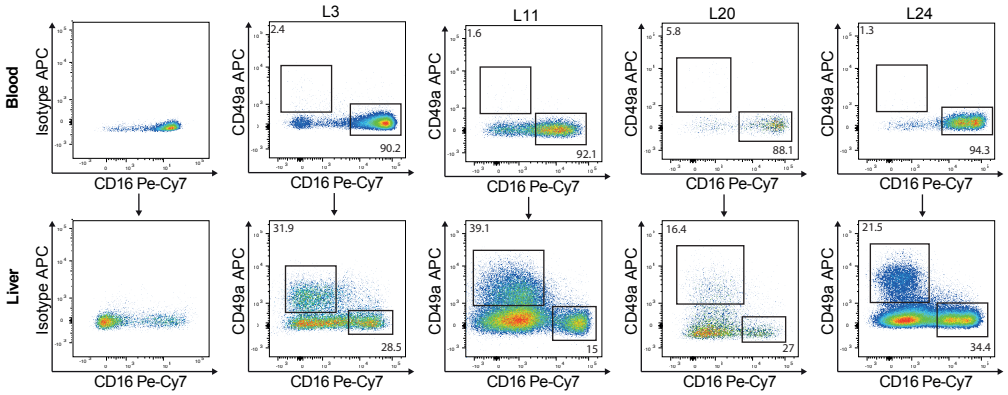

c CD49a+CD16- NK cells by diagnosis

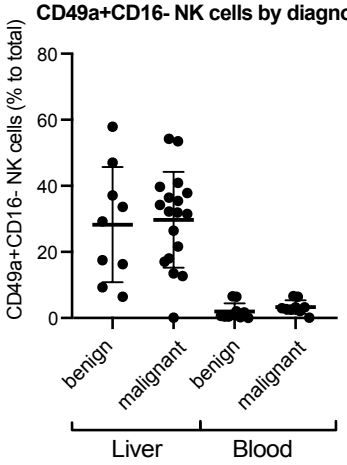

d Single cell RNA-seq on liver CD45+ cells superimposed with expression patterns of known marker genes of CMV driven adaption of NK cells

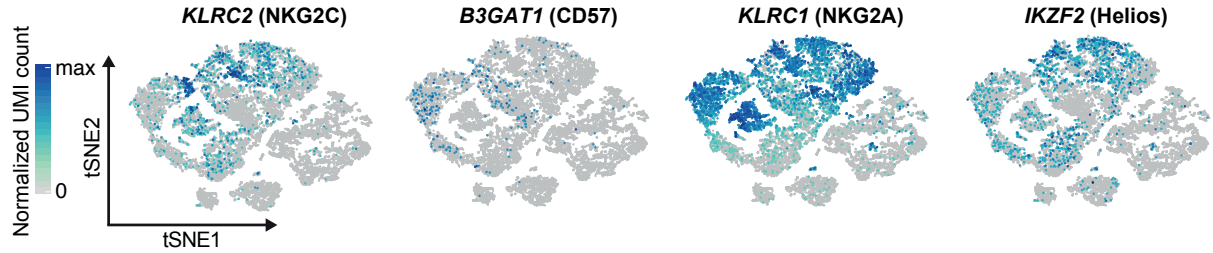

e CD16 and NKG2C expression of NK cells

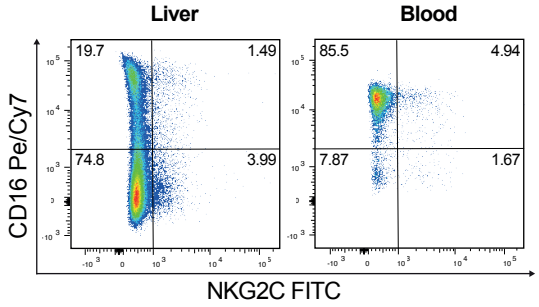

f Mean expression of NKG2C

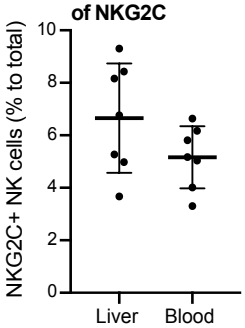

g Markers expressed by NKG2C+ NK cells

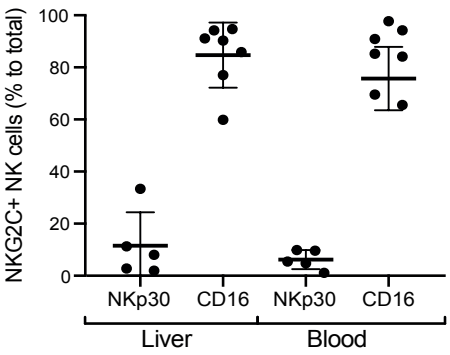

Figure S1. Phenotypic characterization of human liver NK cells**. a**, t-SNE projection of Smart-seq2 single-cell sequencing on human hepatic $CD45^+$ leukocytes superimposed with expression pattern of known marker genes for ILCs. UMI normalized expression of indicated genes within the depicted clusters. **b,** Representative dot plots of stainings of liver- and blood-derived NK cells with anti-CD49a, anti-CD16 and an isotype control. These staining show inter-individual variability with a substantial population of $CD49a^+CD16^-$ NK cells in all liver samples. **c**, Mean percentage of $CD49a^+CD16^-$ NK cells of liver and blood listed according to the diagnosis. **d,** t-SNE projection of Smart-seq2 single-cell sequencing on human hepatic $CD45^+$ leukocytes superimposed with expression pattern of known marker genes for CMV-driven adaptive NK cells. UMI normalized expression of indicated genes within the depicted clusters. **e**, Representative FACS plots of expression of CD16 and NKG2C of NK cells in liver and blood. **f**, Mean percentage of NK cells expressing NKG2C in liver and blood. **g**, Mean percentage of $NKG2C^+$ NK cells expressing depicted markers in liver and blood.

Supplementary Figure 2.

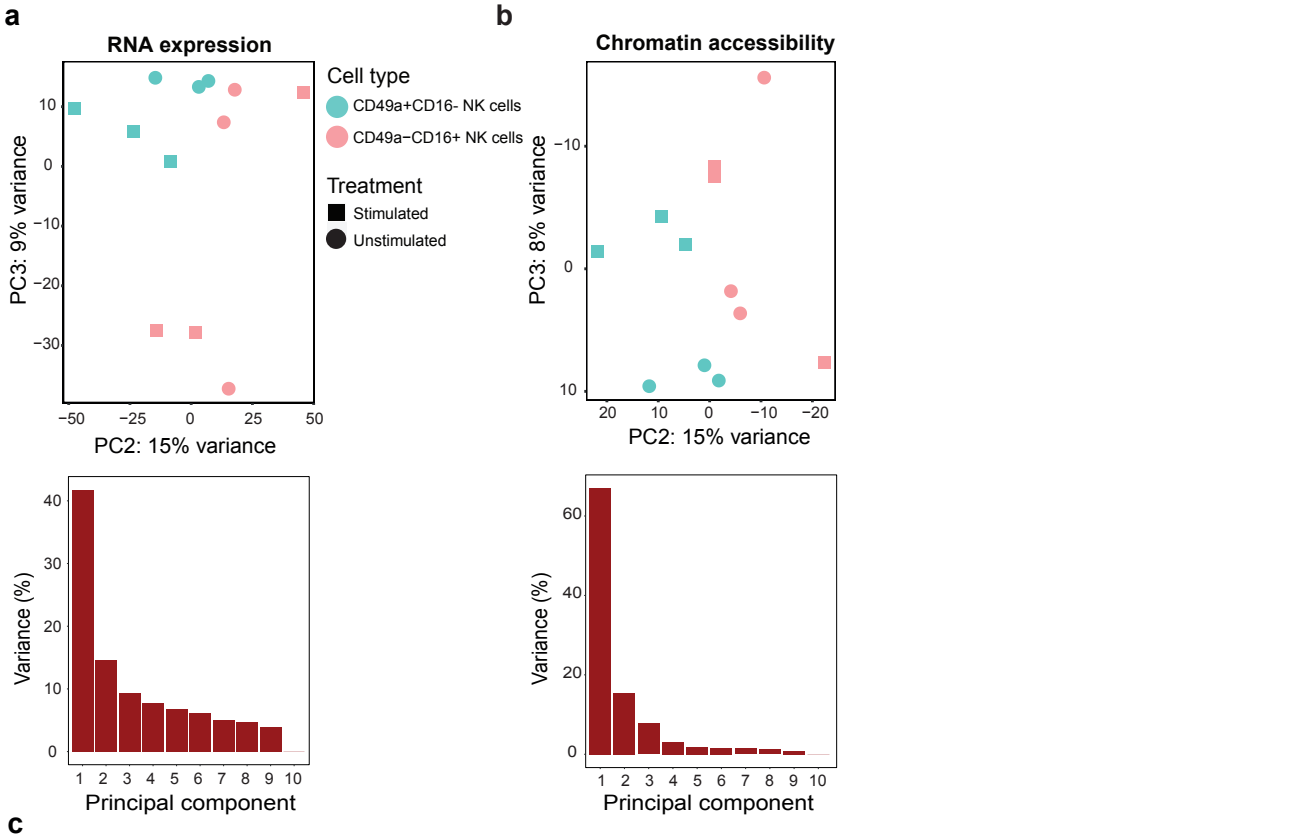

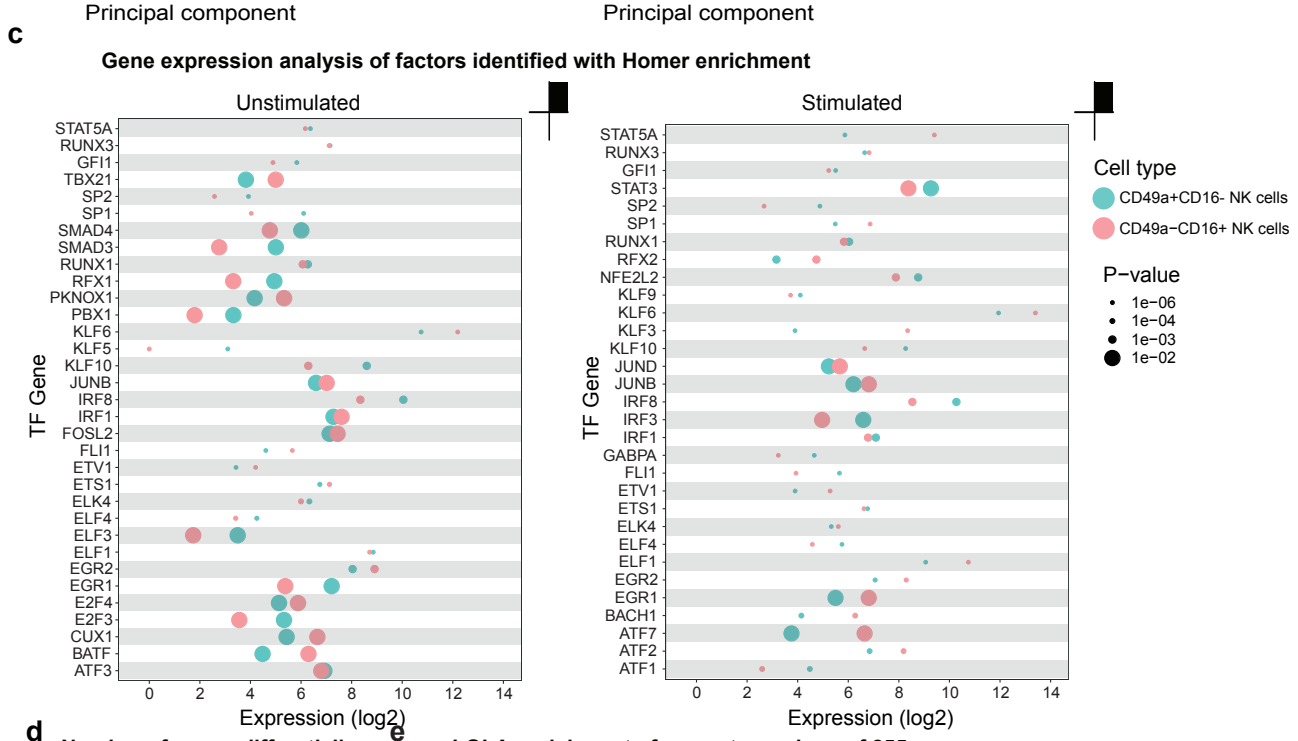

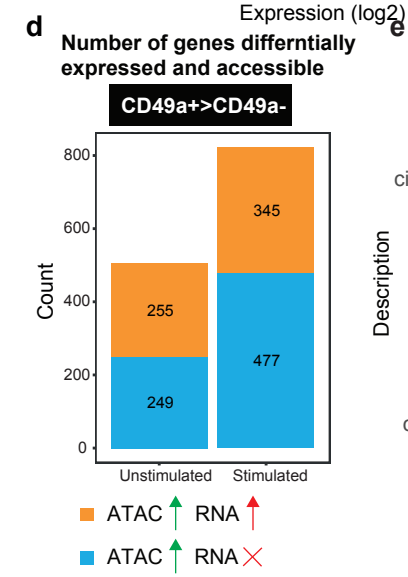

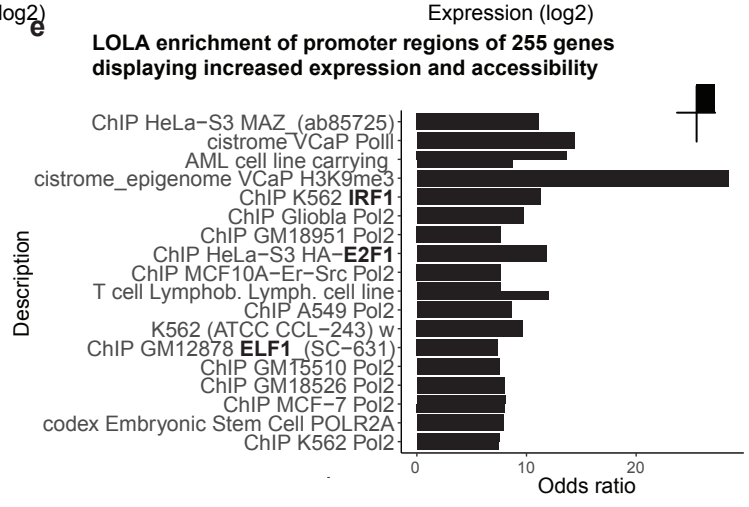

Figure S2. Transcriptomic and epigenomic differences in NK cell subtypes**. a,** PCA analysis with Principal component 2 (PC2) and Principal component 3 (PC3) of the same set of genes as Figure 2a (top). The bar plot (bottom) shows the distribution of 10 principal components. **b**, PCA analysis of ATAC-seq data with Principal component 2 (PC2) and Principal component 3 (PC3) of the same set of differentially accessible (DA) regions as Figure 2b (top). The bar plot (bottom) shows the distribution of 10 principal components. **c,** Transcriptional presence of factors significantly enriched in accessible regions comparing unstimulated and stimulated NK cells and also comparing $CD49a^{+}CD16^{-}$ and $CD49a^{-}CD16^{-}$ NK cells in either unstimulated or stimulated conditions (normalized log2). The size of the circles reflects the HOMER motif enrichment p-values. **d,** Stacked bar plot displaying the number of gained DA peaks at promotor regions in the comparison of $CD49a^{+}CD16^{-}$ NK cells versus $CD49a^{-}CD16^{-}$ NK cells either in unstimulated or stimulated conditions. Peaks associated with upregulated genes (orange color) and peaks without association with up-regulated genes (blue color) **e,** LOLA enrichment analysis for top associated factors on accessible regions with concomitant changes in expression comparing $CD49a^{+}CD16^{-}$ NK cells and $CD49a^{-}CD16^{+}$ NK cells in unstimulated conditions (odds ratio).

Supplementary Figure 3.

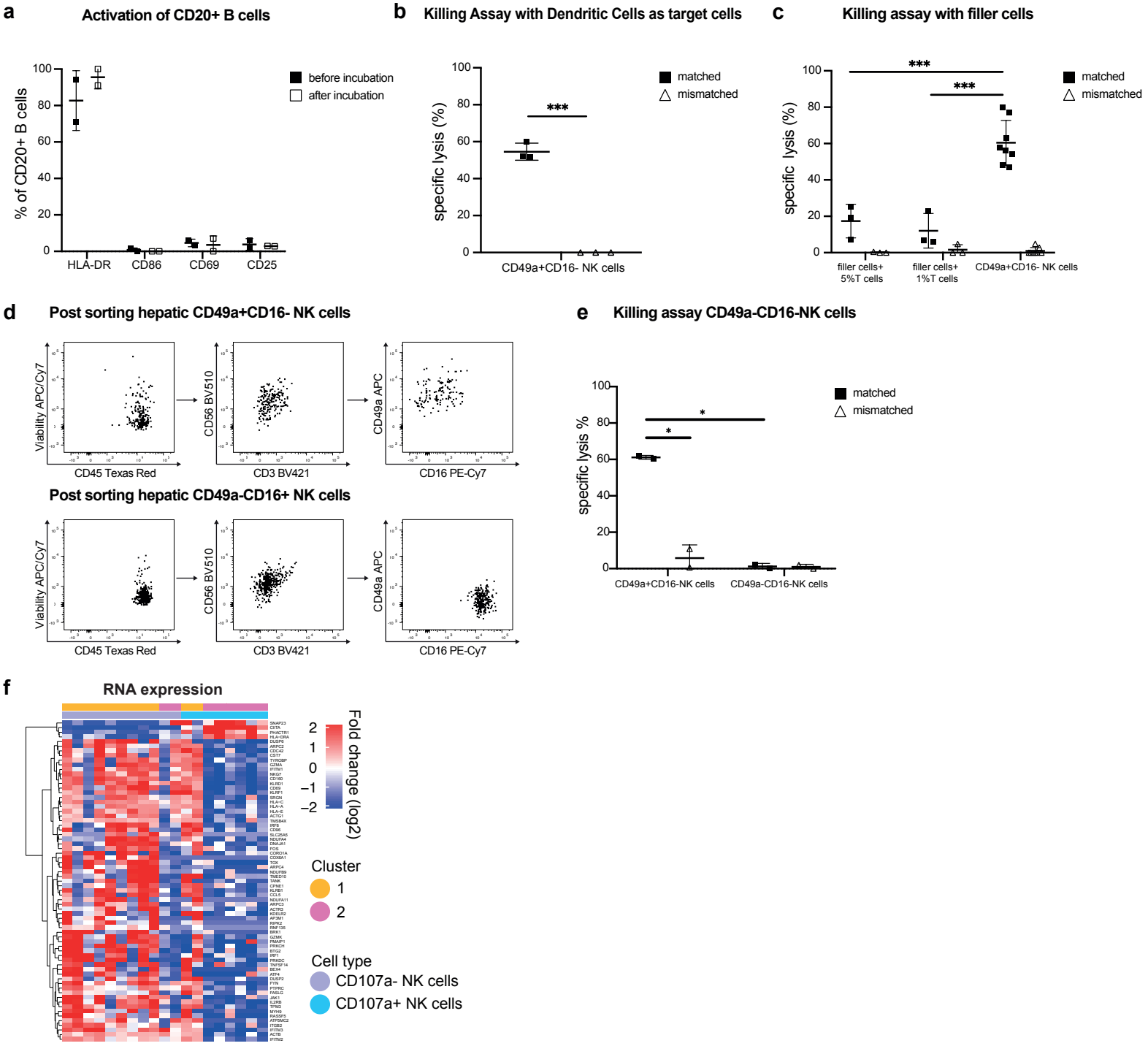

Figure S3. Functional aspects of $CD49a^{+}CD16^{-}$ NK cells**. a,** Mean expression of activation marker on $CD20^{+}$ B cells before and after incubation with antigen proteins. Data points represent the mean of positive B cells ± SD. n = 2. **b**, Antigen-specific lysis of autologous dendritic cells as target cells incubated with matched/mismatched antigens by hepatic $CD49a^{+}CD16^{-}$ NK cells with an effector: target cell ratio of 1:10. n = 3. ***P < 0.0001. **c**, Antigen-specific lysis of autologous B cells pulsed with matched/mismatched antigens by filler cells plus 5% and 1% $CD8^{+}$ effector T cells. This did not lead to a lysis comparable to $CD49a^{+}CD16^{-}$ hepatic NK cells as controls. The effector: target cell ratio was 1:10; n = 3 (filler cells); n = 8 (positive control). ***P < 0.0001. **d**, Representative dot plots post-sorting of $CD49a^{+}CD16^{-}$ NK cells and $CD49a^{-}CD16^{+}$ NK cells. **e**, Antigen-specific lysis of $CD49a^{-}CD16^{-}$ NK cells compared to $CD49a^{+}CD16^{-}$ hepatic NK cells against autologous B cells pulsed with matched/mismatched antigens. The effector: target cell ratio was 1:10; n = 2. *P < 0.01. **f**, Single-cell Smart-seq2 sequencing was performed after an antigen-specific cytotoxicity assay (shown in Fig. 3i). Complete heat map of differentially expressed genes in the two identified clusters of $CD107a^{+/-}$ $CD49a^{+}CD16^{-}$ NK cells (analogous to Fig. 3k).

Table S5. Characteristics of individuals for liver tissue. Data presented as total numbers.

Patient	Age	Gender	Tumor
L1	60	Female	Klatskin tumor
L2	77	Female	Cholangiocellular carcinoma
L3	82	Male	Colorectal carcinoma
L4	46	Female	Hemangioma
L5	54	Male	Neuroendocrine tumor
L6	45	Female	Colorectal carcinoma
L7	37	Male	Adenoma
L8	68	Female	Colorectal carcinoma
L9	73	Female	Angiomyolipoma
L10	65	Male	Hepatocellular carcinoma
L11	39	Female	Adenoma
L12	78	Male	Hepatocellular carcinoma
L13	70	Male	Hepatocellular carcinoma
L14	47	Female	Schwannoma
L15	78	Male	Colorectal carcinoma
L16	62	Male	Hepatocellular carcinoma
L19	58	Female	Liver cysts
L20	75	Male	Colorectal carcinoma
L21	53	Female	Adenoma
L22	69	Male	Cholangiocellular carcinoma
L23	66	Male	Colorectal carcinoma
L24	38	Female	Focal nodular hyperplasia
L25	66	Male	Colorectal carcinoma
L26	75	Male	Hepatocellular carcinoma
L27	76	Male	Hepatocellular carcinoma
L28	58	Female	Liver cysts
L30	45	Female	Cholangiocellular carcinoma

Table S6. Characteristics of individuals with nickel-induced epicutaneous patch test (Ni-ECT). Data presented as total numbers.

Patient	Age	Gender	Grade NI-ECT
1	29	Female	III
2	50	Female	II
3	67	Female	II
4	52	Female	III

Table S7. Antibodies used in this study.

Antibody specificity	Clone (source of antibodies)	Isotype
CD3	UCHT1	IgG1
CD8	SK1	IgG1
CD16	B73.1	IgG1
CD20	2H7	IgG2b
CD45	HI30	IgG1
CD49a	TS2/7	IgG1
CD49b	P1E6-C5	IgG1
CD56	HCD56	IgG1
CD57	HNK-1	IgM
CD69	FN50	IgG1
CD94	DX22	IgG1
CD107a	H4A3	IgG1
CD160	BY55	IgM
CD244	C1.7	IgG1
PD-1	EH12.2H7	IgG1
Siglec7	6-434	IgG1
NKG2A/CD94	131411	IgG2a
NKG2C/CD159c	134522	IgG2a
NKG2D	1D11	IgG1
NKp30	P30-15	IgG1
NKp46	BAB281	IgG1
KIR2DL1/S1/S3/S5	HP-MA4	IgG2b
LIR-1	GHI/75	IgG2b
CCR2	K036C2	IgG2b
CCR3	J073E5	IgG2a
CCR4	1G1	IgG1
CCR5	CTC5R	IgG1
CCR8	L263G8	IgG2a
CCR10	314305	IgG2a
CXCR1	8F1/CXCR1	IgG2b
CXCR2	5E8/CXCR2	IgG1
CXCR3	G025H7	IgG1
CXCR6	K041E5	IgG2a
CXCL16	REA873	IgG1
CLA	HECA-452	IgM rat
EOMES	WD1928	IgG1
T-bet	4B10	IgG1
Interferon-γ	B27	IgG1
IL-4	3010.211	IgG1
IL-17A	N49-653	IgG1
HLA-DR	L243	IgG2a
Ki-67	20Raj1	IgG1